Topic number: 5

Absolute Concentrations of Atomic Radicals in Cold Atmospheric Pressure Plasmas

Kari Niemi(*), Jochen Waskoenig, Lucy Marie Graham, Timo Gans

Centre for Plasma Physics, Queen's University Belfast, Belfast BT7 1NN, Northern Ireland, UK
(*) **k.niemi@qub.ac.uk**

Cold atmospheric pressure plasma jets promise high potential for temperature sensitive surface treatments in biomedicine [1, 2]. A stable homogeneous low temperature plasma operation is achieved by using helium feed gas and applying radio frequency excitation. Small admixtures of molecular oxygen to the feed gas lead to the efficient generation of highly reactive oxygen radicals. A quantification of these radical densities and fluxes is vital for the plasma source development and fundamental understanding.

Diagnostics of atmospheric pressure plasmas are extremely challenging due to small confining structures and the collision dominated high pressure environment demanding exceptionally high spatial and temporal resolution down to microns and picoseconds. Atomic oxygen densities have been measured using two-photon absorption laser-induced fluorescence (TALIF) spectroscopy [3]. This technique is, however, highly intricate and experimentally limited to plasma source designs providing extensive diagnostic access. Simpler less demanding techniques such as model predictions or optical emission spectroscopy are highly requisite. Modeling plasma chemistry at atmospheric pressure is particularly ambiguous due to the multitude of possible reactions with vaguely known or even ill-defined reaction rates, in particular for three-body collisions and surface interactions. A promising approach is active combination of advanced optical techniques and numerical simulations. Diagnostic based modelling [4, 5] as a method to determine absolute atomic oxygen ground state densities inside such atmospheric pressure plasmas is proposed. A one-dimensional numerical simulation yields the spatial and temporal electron dynamics and subsequently the excitation efficiency of optical emission lines which intensities are measured temporally integrated. The population dynamics of the O $3p\,^3P$ ($\lambda = 844$ nm) atomic oxygen state is governed by direct electron impact excitation, dissociative excitation, radiation losses, and collisional induced quenching. Absolute atomic oxygen densities are obtained through comparison with the Ar $2p_1$ ($\lambda = 750.4$ nm) state. Results for spatial profiles and power variations are presented. An excellent quantitative agreement with independent two-photon absorption laser-induced fluorescence measurements [6] is found.

The investigated discharge is a micro-scaled atmospheric pressure plasma jet (μAPPJ) that produces a cold homogeneous α-mode glow discharge at ambient pressure. The setup, see fig. 1, consists of two plane parallel stainless steel electrodes capped with quartz windows along the sides, forming a core plasma channel of 30 mm length and 1 mm $\times$ 1 mm cross section. A fixed feed gas composition is used: 1 slm He with 0.5% O_2 and 0.1% Ar admixtures. The jet is driven at 13.56 MHz with up to 65 W power using an rf broadband amplifier connected to the powered electrode via an impedance matching network. Optical emission spectra of the core plasma are recorded with a sensitivity calibrated spectrograph (430 to 950 nm, 0.5 nm FWHM resolution). The optical emission is collected via an optical fibre perpendicular to the plasma channel through the quartz windows of the jet (1.4 mm effective spatial resolution) to obtain a time and space average across the discharge gap.

The time and space averaged intensity of the selected $\lambda = 844$ nm atomic oxygen emission line resulting from direct electron-impact excitation is given by $\langle I \rangle = h\nu\, a_{ik}\, \langle k_e\, n_e \rangle\, n_{gd}$, where $h\nu$ denotes the photon energy, $a_{ik} = A_{ik}/\sum_j A_{ij}$ the optical branching ratio of the transition, n_e the electron density, n_{gd} the O-atom ground state density. The excitation rate coefficient $k_e = \int f(\varepsilon)\,\sigma(\varepsilon)\,v_e\,\mathrm{d}\varepsilon$ is the convolution of the normalised electron energy distribution function (EEDF) $f(\varepsilon)$, the electron impact excitation cross section $\sigma(\varepsilon)$, and the electron velocity $v_e = \sqrt{2\varepsilon/m_e}$.

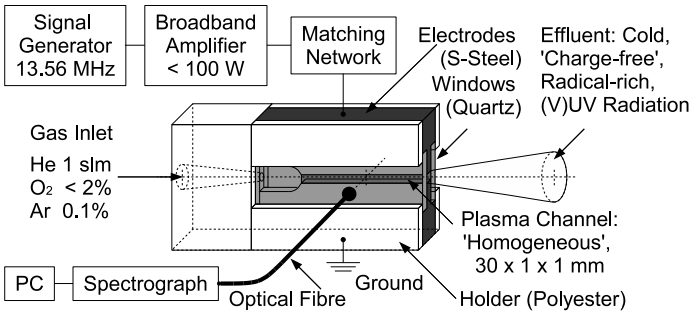

Fig. 1: Schematic of the μ-APPJ.

The observation volume and the solid angle can be accounted for by normalizing the measured optical emission from atomic oxygen to the emission signal from an inert gas admixed as an actinometer gas in defined trace amounts according to the classical actinometry concept [7]. In our case the $\lambda = 750.4\,\mathrm{nm}$ emission line of argon is chosen, which is also primarily excited from the ground state as compared to from metastables or by cascades. Under the assumption that the electron-impact excitation cross sections have the same shape and threshold, the ratio of the excitation rates is independent of the plasma conditions. This approach can provide a qualitative measurement of the atomic oxygen ground state density in low pressure plasmas with not too low degree of dissociation [8]. The determination of absolute O-atom densities in cold atmospheric pressure plasmas is, however, significantly more complex.

Collisional-induced quenching of the upper O($3p\,^3P$) and Ar($2p_1$) states outbalancing the optical transition rates needs to be accounted for. The effective optical branching ratios of the corresponding transitions are calculated on the basis of quenching coefficients [3, 9] for the feed gas composition according to $a_{ik} = A_{ik}/(A_i + \sum_q k_{iq} n_q)$, where k_{iq} denotes the quenching rate coefficient for a collider density n_q. Both latter quantities dependent on the gas temperature, which was measured spectroscopically from N_2 band emission spectra.

The thresholds for direct electron-impact excitation of O($3p\,^3P$) and Ar($2p_1$) differ by 2.5 eV. This difference is critical at atmospheric pressure, since the EEDF varies significantly in this range. The validity of the classical actinometry – a constant ratio of the direct excitation rates – is not given for the chosen emission lines at low mean electron energies typical for atmospheric pressure plasmas, as discussed in [4]. Therefore, it is necessary to determine the pronounced temporal and spatial electron dynamics in detail. Subsequently, the time and space averaged electron density weighted EEDF can be calculated for deriving effective excitation rates according to $k_e^* = \langle n_e \rangle^{-1} \int \langle n_e\, f(\varepsilon) \rangle\, \sigma(\varepsilon)\, v_e\, \mathrm{d}\varepsilon$ to evaluate the integrated OES measurements more reliably. The electron energy distribution function is obtained from a one-dimensional numerical simulation based on fluid equations with a semi-kinetic treatment of electrons. The input data of the model are kinetic reaction rates and transport coefficients calculated as a function of gas mixture and mean electron energy using the two-term approximation Boltzmann solver Bolsig+ [10]. The number of considered species (He, He^*, He^+, He_2^*, He_2^+, O_2, O_2^+) and reactions (17 in total) are purposely kept minimum, since details of the plasma chemistry and resulting atomic oxygen densities are represented in the measured optical emission signal. Since only the slope in the relevant energy range of the excitation thresholds is required, a rather simple numerical simulation of the electron properties without inclusion of chemical reactions is sufficient.

Figure 2a shows the calculated spatio-temporal characteristics of the effective excitation rate coefficient of the Ar($2p_1$) state across the electrode gap over one rf cycle for a voltage amplitude of 245 V. In each half cycle three excitation maxima are observed. The strongest can be attributed to the sheath collapse. The maxima occurring simultaneously indicate the sheath expansion at the opposite electrode. The maximum within the plasma boundary sheath is due to secondary

Topic number: 5

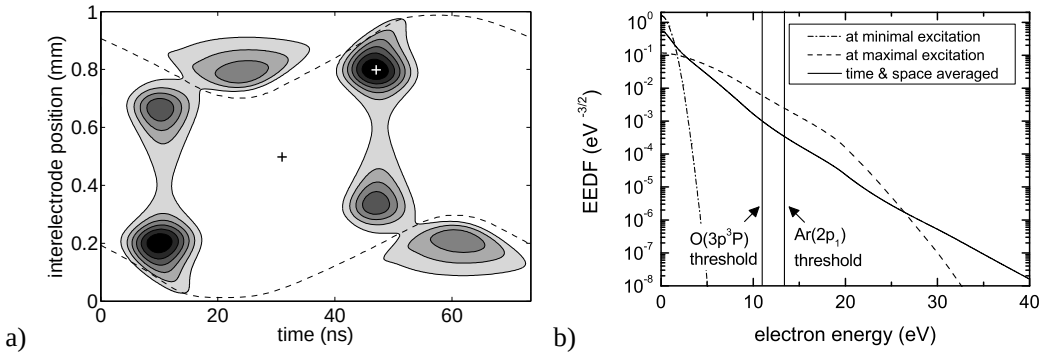

Fig. 2: a) Simulated time and space resolved electron-impact excitation rate coefficient for the Ar($2p_1$) state on a linear gray scale starting from zero. The dashed curves indicate the sheath edges. b) Calculated EEDF. Time and space of minimal and maximal excitation is marked in subfigure a) by crosses.

electron multiplication through high electric fields in this region. The structures of these three excitation mechanisms correspond well to the results of independent simulations [11] and experimental observations [12]. Figure 2b shows the resulting time and space averaged EEDF as well as the temporal and local EEDF at minimal excitation in the bulk region and at maximal excitation in the sheath collapse region. There is a pronounced group of low energy electrons trapped by the ambipolar potential during the whole rf cycle. Excitation and emission are dominantly caused by the midenergy electrons resulting from the sheath heating mechanisms. These features are in agreement with results of particle-in-cell simulations [13].

The effective excitation rate coefficients k_e^*, adequately describing the time and space integrated optical emission measurements, are calculated to be $k^*_{Ar,e}/k^*_{O,e} = 0.32$ and $k^*_{O,de}/k^*_{O,e} = 9\times10^{-3}$. The indices e and de denote direct and dissociative excitation, respectively. The difference in the ratios of whether chemical reactions are included in the model or not is below 3%. The O-atom density is finally evaluated according to

$$n_O = \frac{I_O}{I_{Ar}}\frac{h\nu_{Ar}}{h\nu_O}\frac{k^*_{Ar,e}}{k^*_{O,e}}\frac{a_{Ar}}{a_O}\,n_{Ar} - \frac{k^*_{O,de}}{k^*_{O,e}}\,n_{O2}\,, \qquad (1)$$

where a_{Ar} and a_O denote the effective optical branching ratios of the observed transitions, as introduced above. On the right hand side of equation 1, the first term is formally equal to the classical actinometry approach, while the second term represents the dissociative channel correction.

The derived atomic oxygen densities in the centre of the plasma channel as a function of applied rf power are shown in figure 3a. The plasma ignites at 25 W input power and spreads over the entire electrode length. Once ignited, the plasma can be sustained down to 18 W. The O-atom density increases linearly with power from $0.8\times10^{16}\,\mathrm{cm}^{-3}$ to $1.4\times10^{16}\,\mathrm{cm}^{-3}$ at 50 W. At higher powers, the plasma no longer operates in a pure α-mode. Additional electrons are generated near the electrode surface by the γ-effect as well as by Penning ionization from (He^*, He_2^*) metastables and the O-atom density increases overlinearly with power. At a power of about 65 W, the plasma switches to a spatially constricted mode with a high current density.

Figure 3b shows the atomic oxygen density along the plasma channel (nozzle at zero position, gas inlet at 30 mm). The atomic oxygen density increases from about $1.4\times10^{16}\,\mathrm{cm}^{-3}$ over a distance of 10 mm, approaching a constant value of about $1.7\times10^{16}\,\mathrm{cm}^{-3}$, indicating that the destruction and production processes of atomic oxygen balance. This equilibrium is reached after 0.6 ms, correspondent to the gas velocity of about $17\,\mathrm{ms}^{-1}$. The 750 nm argon line intensity probing the electron properties remains constant after the first 2 mm of the discharge, after 0.12 ms correspondingly, indicating that the core plasma is homogeneous. At 10 mm distance to the nozzle the O-atom density as well as the argon emission starts decreasing. This effect is most likely

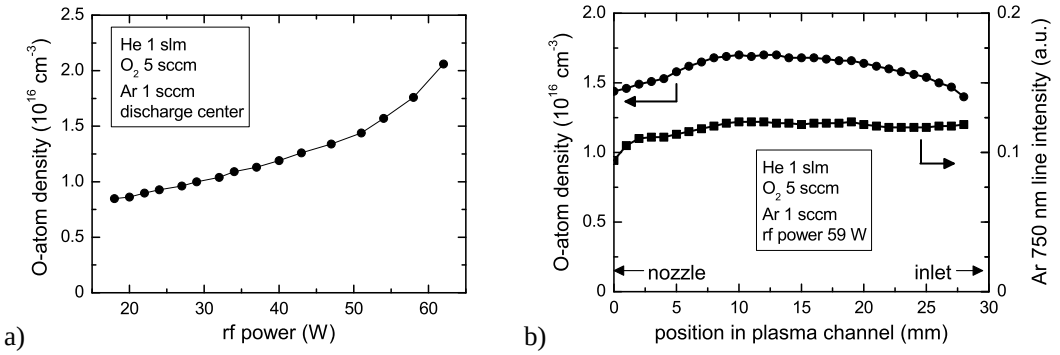

Fig. 3: a) O-atom density in the discharge center as a function of rf generator power. b) O-atom density and Ar 750 nm emission line intensity along the discharge channel.

caused by ambient air species backdiffusing from the nozzle into the plasma. The resulting atomic oxygen densities are quantitatively consistent with independent TALIF measurements on a similar setup [6].

Acknowledgments

The authors acknowledge support by a Science and Innovation Award of the EPSRC. One author (L.M.G) is supported by DEL. We thank N Knake and V Schulz-von der Gathen (Ruhr-Universität Bochum) for valuable discussion as well as S Reuter for his help with intial measurements. The numerical simulations have been generously supported by Y Sakiyama and D B Graves (University California Berkeley).

Reference

[1] E. Stoffels, I. E. Kieft, R. E. J. Sladek, L. J. M. van den Bedem, E. P. van der Laan and M. Steinbuch, 2006 Plasma Sources Sci. Technol. **15** S169
[2] R. Foest, E. Kindel, L. Lange, A. Ohl, M. Stieber and K.-D. Weltmann 2007 Contrib. Plasma Phys. **47** 119
[3] K. Niemi, V. Schulz-von der Gathen and H. F. Döbele 2005 Plasma Sources Sci. Technol. **14** 375
[4] K. Niemi, S. Reuter, L. M. Graham, J. Waskoenig and T. Gans, 2009 Appl. Phys. Lett. **95** 151504
[5] K. Niemi, S. Reuter, L. M. Graham, J. Waskoenig, N. Knake, V. Schulz-von der Gathen and T. Gans, 2010 J. Phys. D: Appl. Phys. **43** 124006
[6] N. Knake, K. Niemi, S. Reuter, V. Schulz-von der Gathen and J. Winter, 2008 Appl. Phys. Lett. **93** 131503
[7] J. W. Coburn and M. Chen 1980 J. Appl. Phys. **51** 3134
[8] R. E. Walkup, K. L. Saenger and G. S. Selwyn 1986 J. Chem. Phys. **84** 2668
[9] N. Sadeghi, D. W. Setser, A. Francis, U. Czarnetzki and H. F. Döbele 2001 J. Chem. Phys. **115** 3144
[10] G. J. M. Hagelaar and L. C. Pitchford 2005 Plasma Sources Sci. Technol. **14** 722
[11] J. J. Shi and M. G. Kong, 2005 J. Appl. Phys. **97** 023306
[12] V. Schulz-von der Gathen, L. Schaper, N. Knake, S. Reuter, K. Niemi, T. Gans, and J. Winter, 2008 J. Phys. D: Appl. Phys. **41** 194004
[13] F. Iza, J. K. Lee, and M. G. Kong, 2007 Phys. Rev. Lett. **99** 075004